GeoScienceWorld
Lithosphere
Volume 2022, Article ID 7760591, 18 pages
https://doi.org/10.2113/2022/7760591

Lithosphere

Research Article

Integrated Diagenesis Study of Tight Gas Sandstone: The Permian Lower Shihezi Formation, Northern Ordos Basin, China

Qinghai Xu,[1] **Xiangyang Xie**,[2] **Changmin Zhang**,[1] **Lianfu Hai**,[3] **and Arthur Busbey**[2]

[1]*School of Earth Science, Yangtze University, Wuhan 430100, China*
[2]*Department of Geological Sciences, Texas Christian University, Fort Worth, TX 76129, USA*
[3]*Mineral Geological Survey Institute of Ningxia Hui Autonomous Region, Yinchuan 750021, China*

Correspondence should be addressed to Xiangyang Xie; x.xie@tcu.edu

Received 13 December 2021; Accepted 14 July 2022; Published 25 July 2022

Academic Editor: Vincent Heesakkers

Diagenesis varies greatly from basin to basin and has been considered as the key control of the reservoir quality of tight sandstones. In this study, we analyzed the petrographic characteristics, diagenesis, and pore types and characteristics of the Permian Lower Shihezi Formation in the Ordos Basin. Results show that most of sandstones are litharenites with minor sublitharenites and feldspathic litharenites. The tight sandstones have ultralow permeabilities (averaging 0.67 mD) and porosities (averaging 8.35%), with pore-throat sizes ranging from 0.035 to 13.29 μm with 94.12% less than 5 μm. Overall, the tight sandstone reservoirs have undergone complex diagenetic alteration. Compaction and clay mineral cements are the two crucial diagenetic factors that controlled the tightness of the reservoirs. The compaction destroyed most of primary porosity, and the effective pores are mainly dissolved micropores, intragranular dissolved micropores, and micropores in clay minerals and mineral grains. The chlorite coating might have helped preserve a certain amount of porosity, but pore-lining chlorites significantly obstructed pore throats and reduced permeability. Results of the study provide insights and direct implications for the future success of exploration and production of the tight gas sandstone in the Ordos Basin and other similar tight sandstone reservoirs.

1. Introduction

Theoretically, tight sandstones refer to those which have been deeply buried and have undergone complicated diagenetic alteration [1–5]. In recent decades, tight sandstone gas has become an important unconventional hydrocarbon resource and has contributed to the substantial growth of global hydrocarbon production because of advances in recovery technology [6–10]. Diagenesis has been considered as one of key controls of reservoir quality and potential of tight sandstone gas exploration [11–15], but tight sandstones vary greatly in different fields and basins in terms of generating mechanisms and controlling factors.

This integrated diagenesis study of the Shihezi Formation helps document its reservoir characteristics and forming mechanisms. Several upper Paleozoic tight sandstone gas fields have been discovered on the northern slope of the Ordos Basin since the 1980s [11, 15, 16]. Previous studies have focused on the tectonic evolution, regional geology, sedimentology, and the reservoir properties of upper Paleozoic formations [17–19]. Only limited and local diagenetic studies of those upper Paleozoic tight sandstones have been reported [20–23]. There is a lack of systematic study of diagenesis and its control on the reservoir quality of upper Paleozoic Permian tight sandstones in the Ordos Basin [24, 25].

In this study, we chose the Permian Lower Shihezi Formation, in the Hangjinqi area of northern Ordos Basin, to document its diagenetic characteristics through a combination of thin sections, mercury intrusion capillary pressure (MICP), scanning electron microscope (SEM), X-ray diffraction (XRD), and cathode luminescence (CL) testing. The main objectives include the following: (1) analyzing reservoir compositions, diagenetic events and history, and pore systems; (2) revealing favorable reservoir characteristics; and (3) elucidating main controlling factors on reservoir

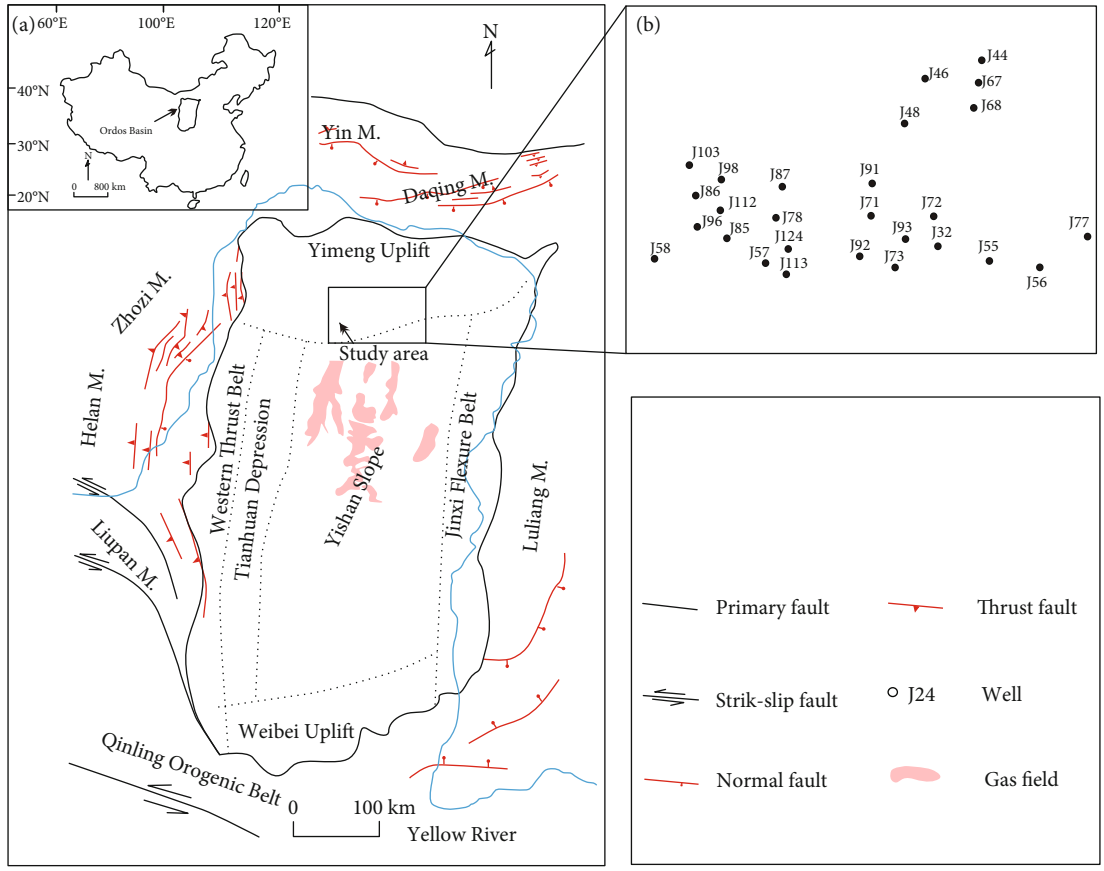

FIGURE 1: The study area location and major tectonic units of the Ordos Basin. (a) The location of Ordos Basin and the study area. (b) The well locations used in this paper.

quality of these tight sandstones. Understanding the diagenetic progress and its effects on reservoir quality can provide important references for favorable reservoir prediction in tight sandstones.

2. Geological Setting

The Ordos Basin is a typical cratonic depression located in North-Central China. Internally, it can be subdivided into six tectonic units: the Yimeng Uplisft, the Western Thrust Belt, the Tianhuan Depression, the Yishan Slope, the Jinxi Flexture Belt, and the Weibei Uplift (Figure 1). The basin has Archean–Proterozoic metamorphic basement and is filled with Paleozoic to Cenozoic aged sedimentary units, with a total thickness of over 4000 meters to the southwest (Figure 2). It experienced six tectonic stages, including (1) Archean to Paleoproterozoic basement formation stage, (2) the Meso- to Neoproterozoic formation of an intracratonic rifting trough (or depression trough), (3) formation of a Sinian to early Paleozoic epicontinental basin on the North China block, (4) Late Paleozoic to early Mesozoic depression of the North China Block, (5) formation of the Middle to late Mesozoic great Ordos inland basin, and (6) formation of a peripheral fault basin.

The study area is in the Hangjinqi region, the border between the Yimen Uplift and the Yishan Slope, in the northern Ordos Basin (Figure 1). In the Hangjinqi area, the basement is directly overlain by the Upper Carboniferous, coal-bearing Taiyuan Formation [26] (Figure 2). Permian to Triassic strata, including the Shanxi, the Lower Shihezi, the Upper Shihezi, the Shiqianfeng, the Liujiagou, the Heshanggou, the Ermaying, and the Yanchang formations (in ascending order), are composed of alluvial fan, deltaic, and lacustrine deposits [27–29]. In the Hangjinqi area, the Late Triassic to Early Jurassic strata are either eroded or missing due to uplift related to Early Jurassic subduction along the eastern margin of Asia [26]. The Middle Jurassic strata, including the Yan'an, the Zhiluo, and the An'ding formations, are mainly fluviolacustrine clastic deposits [30]. The Early Cretaceous strata (the Zhidan Formation) are characterized by fluvial and eolian red beds overlain by Quaternary loess deposits [31, 32]. This region lacks upper Cretaceous-Neogene strata [26, 33].

Two hydrocarbon systems, a Jurassic-Triassic petroleum system and a Paleozoic gas system, exist in this basin [34]. The Paleozoic gas system is mainly found in northern Ordos Basin. Within the Paleozoic gas system, coals from the Taiyuan and Shanxi formations serve as source rocks. Lacustrine mudstones of the Shiqianfeng Formation and Upper Shihezi Formation are the main cap rocks. Deltaic sandstones of the Shanxi and the Lower Shihezi formations are the main reservoir rocks (Figure 2). This study is mainly

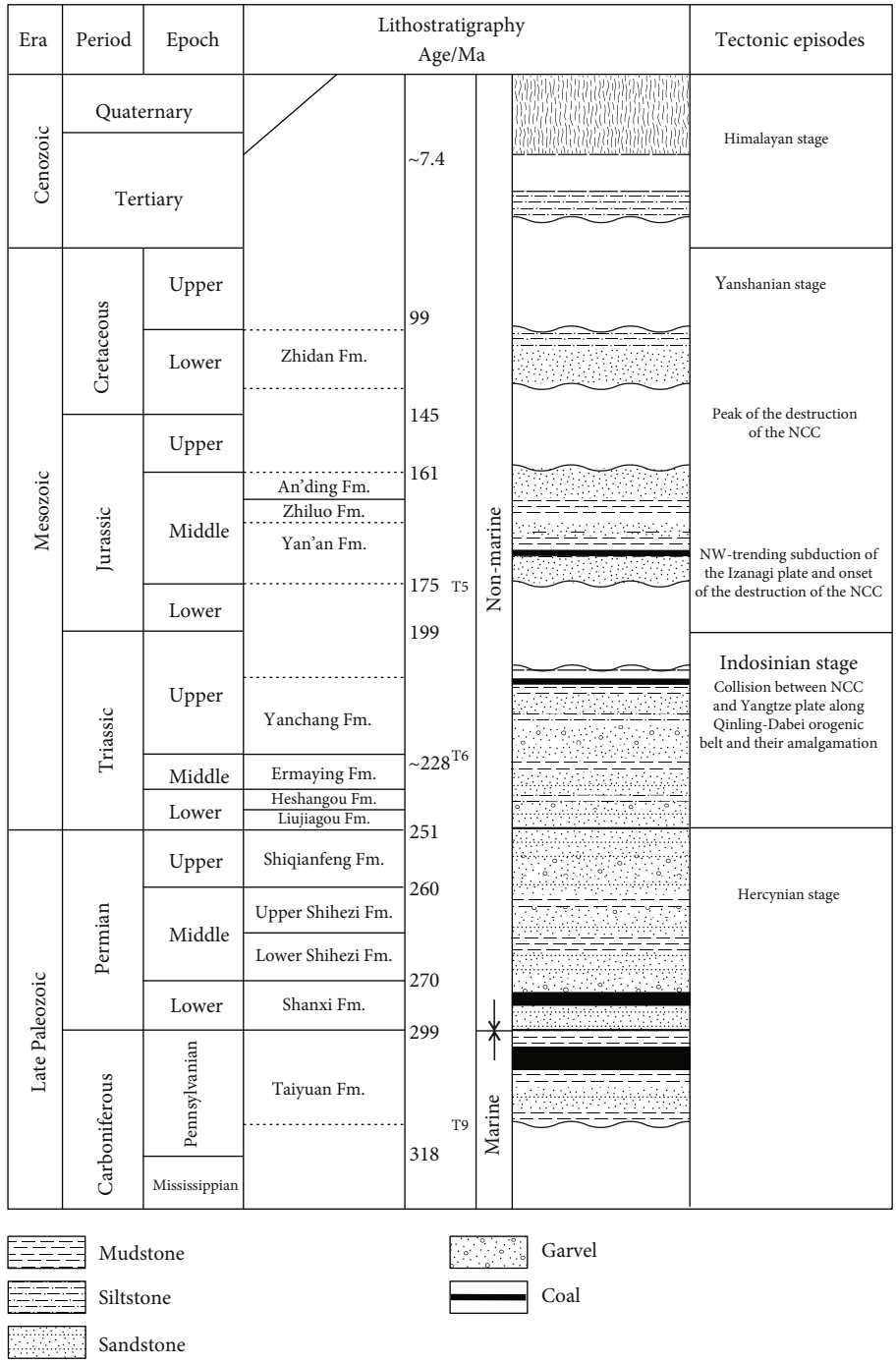

Figure 2: Simplified regional stratigraphic succession and tectonic history of the Hangjinqi area, Ordos Basin.

focused on sandstones of the Lower Shihezi Formation. This area experienced multiple burial events and two main uplifts after the deposition of the Lower Shihezi Formation (Figure 3). The first uplift after depression developed during the Jurassic with an average burial depth of about 2500 m, with the formation temperature reaching 90°C to 100°C [35]. The second uplift developed in the Late Cretaceous with an average burial depth of about 3000 m with the formation temperature reaching 115°C to 130°C [36]. The modern burial depth is about 2000 m to 3000 m with formation temperatures from 85°C to 95°C.

3. Methods and Data

We observed and described cores from 22 wells and collected 110 tight gas sandstone plugs (2.5 cm in diameter and 5 cm in length). 110 standard thin sections were used to analyze grain size, and a total of 110 polished thin sections

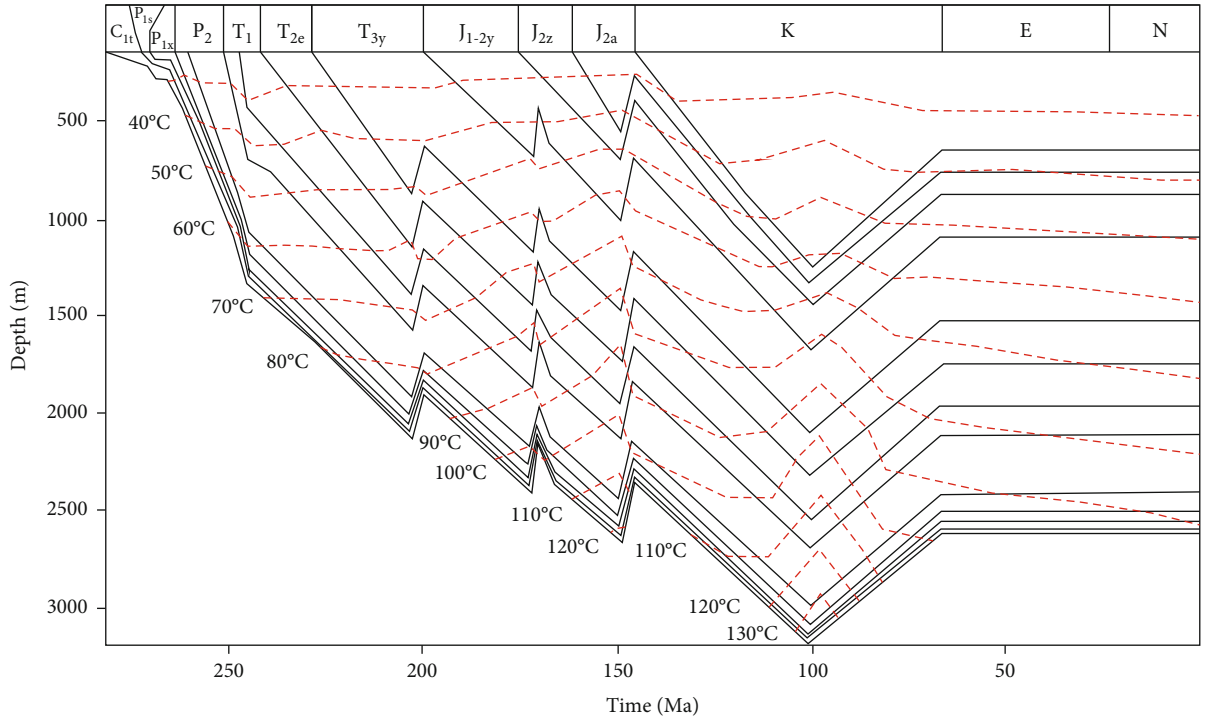

Figure 3: Burial history and paleogeothermal field evolution of study area (changed from [37]).

Table 1: The wells, test types, and numbers.

Well	Plugs	Thin sections	Polished thin sections	SEM	MICP	CL	XRD
J58	6	6	6	4	4	4	4
J96	5	5	5	/	5	/	/
J86	5	5	5	/	5	/	/
J98	5	5	5	4	4	4	4
J112	5	5	5	/	/	/	/
J85	5	5	5	5	5	2	2
J57	5	5	5	/	/	/	/
J124	5	5	5	5	5	2	2
J78	5	5	5	/	5	/	/
J87	5	5	5	3	3	2	2
J92	5	5	5	4	4	2	2
J91	5	5	5	/	5	/	/
J73	5	5	5	/	5	/	/
J93	5	5	5	/	5	/	/
J32	5	5	5	/	/	/	/
J72	5	5	5	3	3	2	2
J48	5	5	5	/	/	/	/
J46	4	4	4	4	4	4	4
J44	5	5	5	/	5	/	/
J55	5	5	5	4	4	4	4
J56	5	5	5	/	5	/	/
J77	5	5	5	4	4	4	4

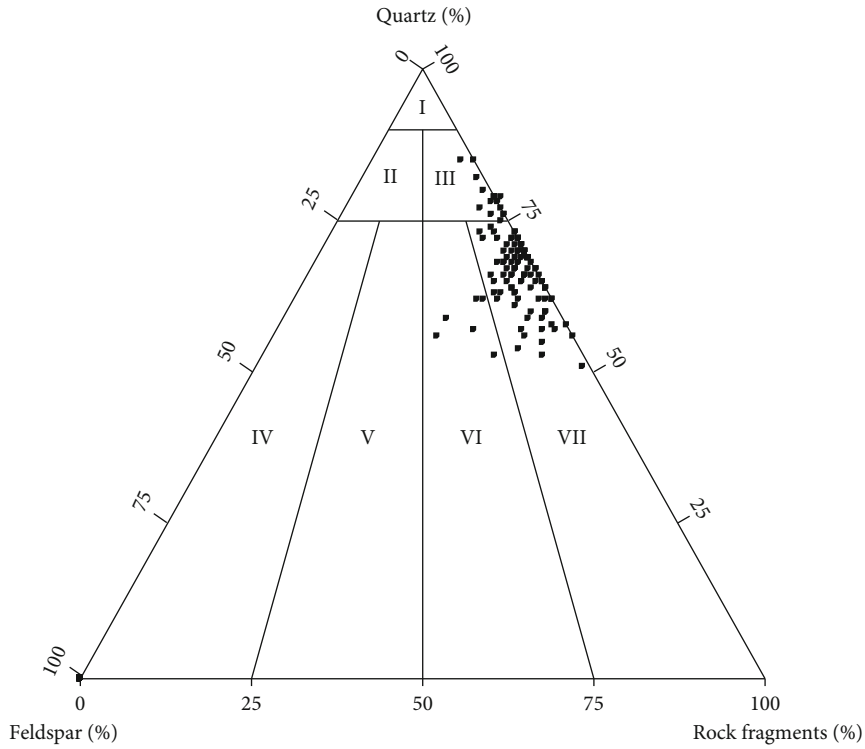

Figure 4: Composition of the Lower Shihezi sandstones.

were utilized to study mineral composition, diagenesis, and pore characteristics. Scanning electron microscopy (SEM) of 40 samples and mercury injection capillary pressure (MICP) analyses from 86 core plug samples were applied to study pore throat structure, observe the mineralogy, and document diagenetic events. Cathodoluminescence (CL) and X-ray diffraction (XRD) analyses of 30 samples were also used to identify and evaluate the mineral content. Additionally, results of porosity and permeability analyses of 1188 samples from cores of 11 wells and 86 samples of MICP were conducted by the Research Institute of China Sinopec North China Company (RICSNCC) and were incorporated into this study to further evaluate the storage and potential of reservoirs. The test types and numbers are listed in Table 1 as follows and well locations in Figure 1(b).

4. Results

4.1. Composition. The results of 115 thin sections show that the Lower Shihezi sandstones are mainly litharenite with minor sublitharenite and feldspathic litharenite according to the sandstone classification of Folk et al. [37] (Figure 4). Framework grains include 51-81% quartz (average~67%), 16-48% rock fragments (average~30%), and less than 10% feldspar (average~ 3%) (Figure 5). Core observation and grain size analyses show that Lower Shihezi tight sandstones range from pebble coarse sandstone, coarse sandstone, to fine sandstone (Figure 5) and are poorly to well-sorted with subrounded to rounded grain shape. There are also small amounts of conglomerate and siltstone.

4.2. Diagenesis. The Lower Shihezi tight sandstones have experienced significant diagenetic modification, including compaction, cementation, alteration and precipitation of clay minerals, and dissolution of quartz and feldspar.

4.2.1. Compaction. Stable packing positions or breakage show strong mechanical compaction (Figures 4(a) and 4(b)), and some grains may have undergone ductile deformation (Figure 5(c)). Concave-convex contacts between detrital grains suggest that chemical compaction was very common, and stylolites were occasionally observed (Figures 5(a)–5(d)).

4.2.2. Clay Mineral Cementation. Four main clay minerals, kaolinite, illite, chlorite, and mixed-layer illite/smectite, were identified based on the SEM morphological characteristics and XRD mineralogical analysis. The content of total clay minerals ranges from 9.9% to 57% with an average of 21.35% in all the tight sandstone samples (Figure 6). In all tested tight sandstone samples, chlorite is the most abundance compared to the other clay minerals clay with averages of 8.62%. And the kaolinite has an average content of 5.49%, the illite-smectite complex has an average content of 4.63%, and illite has an average content of 2.60%.

Most of the authigenic kaolinite occur as vermiculite booklets stacked as pseudohexagonal crystals (Figure 7(a)). The illite mainly occurs as flaky (Figure 7(b)) and fibrous types (Figures 7(d) and 7(f)). There are two types of authigenic chlorite: the pore filling type and the coating type (Figure 7(e)). There is no authigenic quartz where the chlorite coating developed. The flaky illite mainly occurs as pore-filling habits, and fibrous illite mainly surrounds detrital

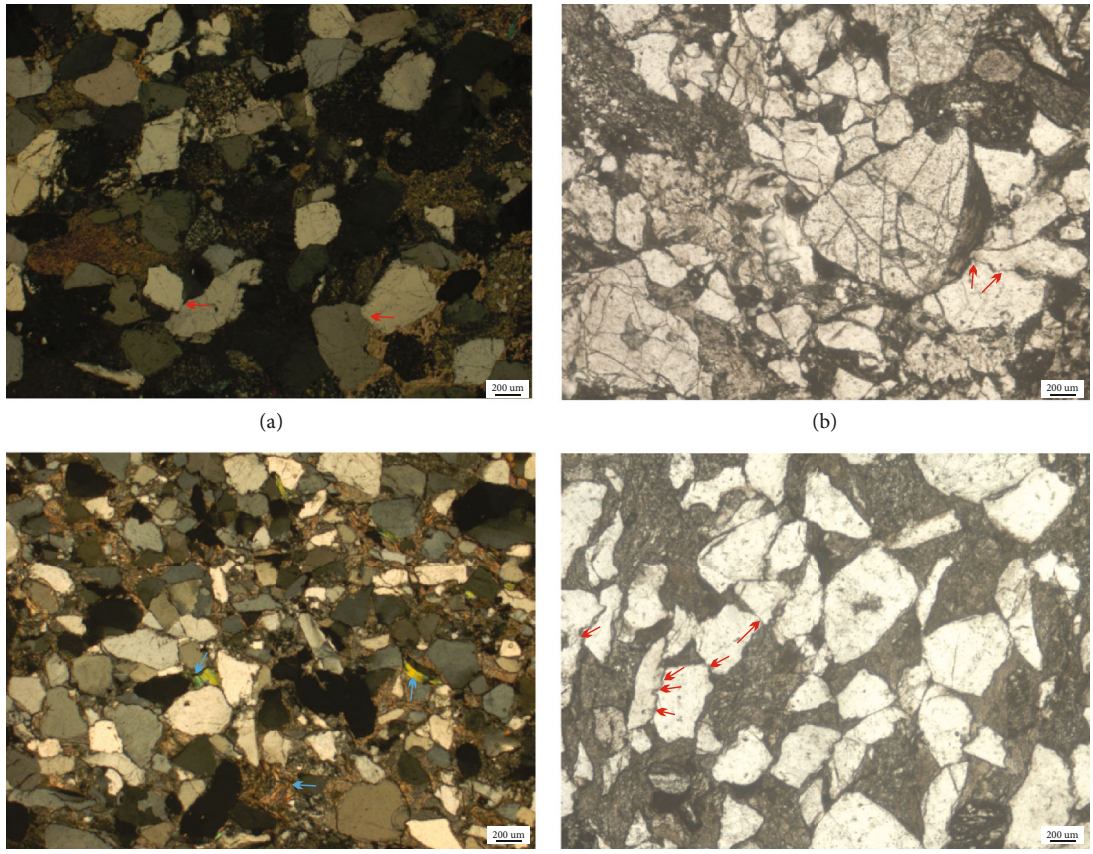

Figure 5: Micrograph of thin section showing grain size and compaction. (a) Grain contacts presenting the linear and concave-convex types (red arrows), and some grains were cracked. Crosspolarized light (CPL), well J107, 3074.67 m. (b) Some grains were cracked and grain contacts presenting the linear and concave-convex types (red arrows). Plane-polarized light (PPL), well J105, 2251.14 m. (c) Mica undergone ductile deformation (blue arrows). CPL, well J30, 3556.33 m. (d) Grain contacts presenting the linear and concave-convex types (red arrows). Detrital components composed quartz and rock fragments with no feldspar. PPL, well J98, 3086.43 m.

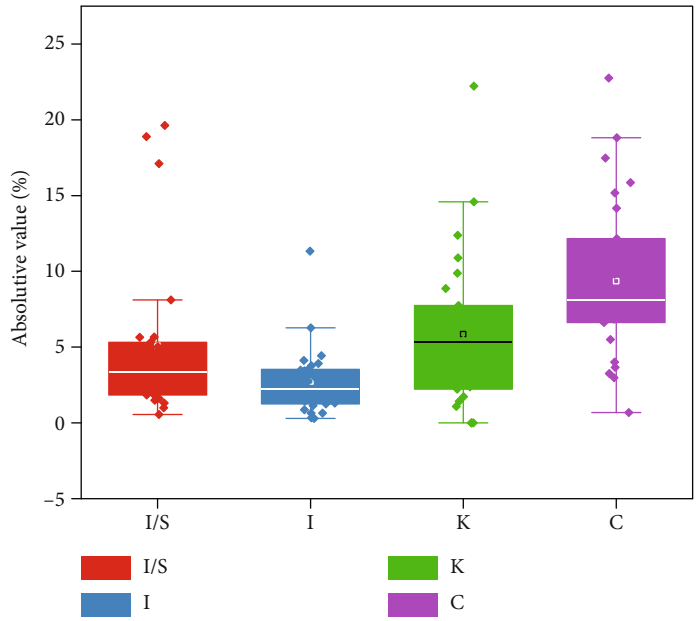

Figure 6: XRD analyses of clay minerals analysis of the selected Lower Shihezi Formation tight sandstone samples from northern Ordos Basin. Key: mixed-layer I/S: illite/smectite; I: illite; K: kaolinite; C: chlorite.

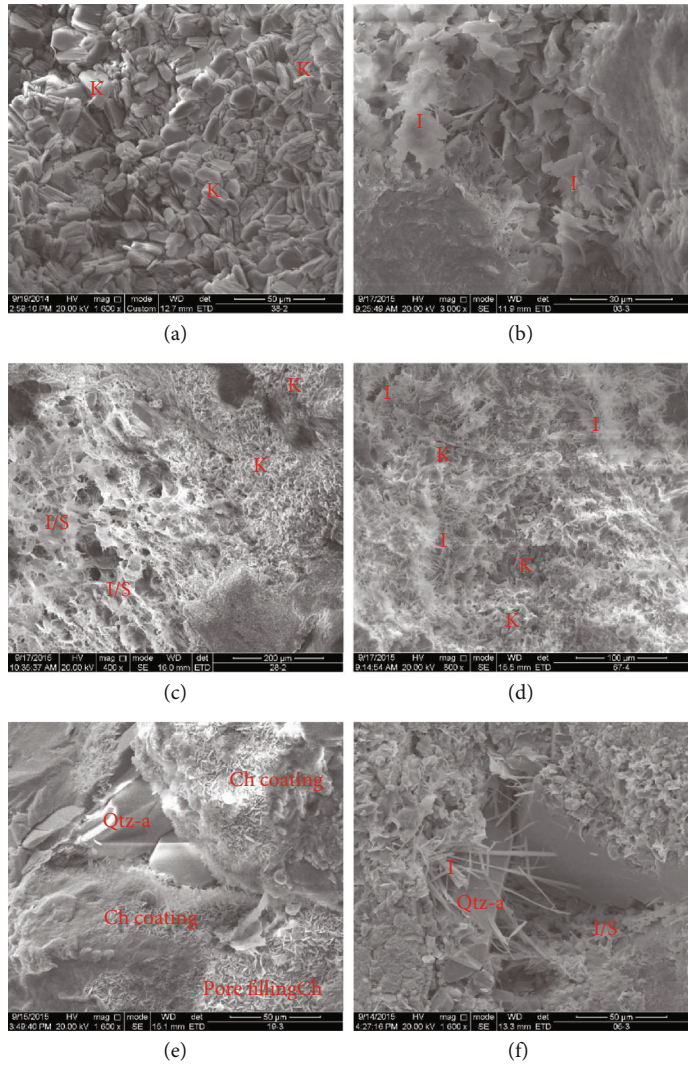

Figure 7: Micrograph of SEM showing the clay mineral cements. (a) Pore-filling authigenic kaolinite grains with booklets of vermicularly stacked morphologies. Well J100, 2931.22 m. (b) Pore-filling authigenic illites occur as flaky type. Well J114, 3007.13 m. (c) Pore-filling I/S and authigenic kaolinite. Well J114, 3023.4 m. (d) Pore-filling authigenic illites and kaolinite. Well J103, 3088.98 m. (e) Two types of authigenic chlorite: the pore filling type and coating type. The chlorite coating developed area has no authigenic quartz. Well J100, 3062.30 m. (f) Authigenic fibrous illite and I/S surround the grains. Well J95, 3086.65 m.

grains or kaolinite, indicating that the illite was formed after the kaolinite.

4.2.3. Quartz Cementation. Quartz cementation is another most common cement in the Lower Shihezi tight sandstones. There are two types of quartz cement. Type I is quartz overgrowths formed by syntaxial overgrowth which partially covers detrital quartz grains and fills in their adjacent intergranular pores (Figures 8(a) and 8(b)). It can be easily differentiated from detrital quartz grains based on dust rims seen under plane-polarized and orthogonal-polarized light (Figure 8(a)). Type II is authigenic quartz crystals that form euhedral overgrowths with complete facets and clear crystal edges and sometimes completely fill primary or secondary pores (Figure 8(d)). This type of quartz cement can be easily distinguished from detrital quartz by using the SEM (Figures 8(d) and 8(f)) and the CL images that show bright luminescence (blue) and authigenic quartz that is nonluminescent (Figures 6(e)and 8(c)). In general, authigenic quartz is approximately 20-100 μm in size (Figures 8(a)–8(d)), and quartz overgrowths often develop where clay rims are discontinuous or missing.

4.2.4. Carbonate Cementation. There are only minor carbonate cements in the Lower Shihezi tight sandstones. Quantitative analyses of the XRD show calcite cements range from 0.0 to 11.4% (average 4.63%). Calcite cements can be easily identified by their purplish red color under the microscope when stained with Alizarin Res S and K-ferricynide (Figure 9(a)) and a reddish orange luminescence color in CL images (Figure 9(b)). Overall, the calcite mainly occurs as pore-filling cements (Figures 9(c) and 9(d)). No dolomite has been observed in any samples.

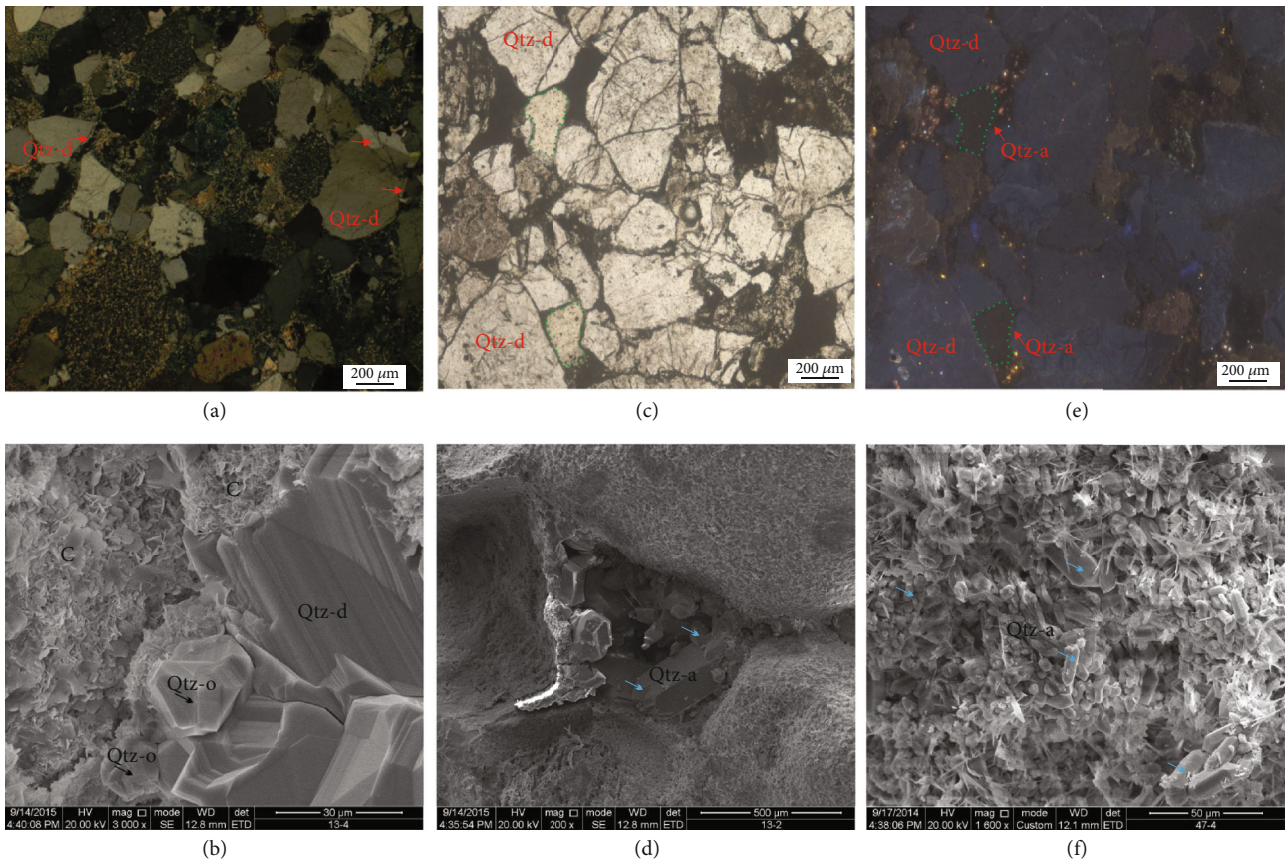

FIGURE 8: Photomicrograph showing quartz cement. (a) Micrograph of thin section showing quartz overgrowth of stage I (red arrows), well J72, 2957.03 m. (b) Micrograph of SEM showing quartz overgrowth which is limited by chlorite grain coating, well J95, 3113.39 m. (c) Micrograph of thin section hard to identify the quartz cement, well J95, 3086.65 m. (d) Micrograph of SEM showing authigenic quartz filled the intergranular pores, well J95, 3114.57 m. (e) Idem with E, but CL micrograph showing the detrital quartz (brightly luminescent) and quartz cement (nonluminescent), well J95, 3086.65 m. (f) Micrograph of SEM showing authigenic quartz, well J97, 2331.66 m. Key: Qtz-d: quartz detrital; Qtz-o: quartz overgrowth; Qtz-a: authigenic quartz crystals; C: chlorite.

4.3. Reservoir Properties

4.3.1. Porosity and Permeability. Tight sandstone reservoirs refer to reservoirs with a porosity of ≤10%, and in-situ formation permeability of ≤0.1 mD or air permeability of ≤1 mD [16, 38]. In this study, we collected porosity and permeability from a total of 1188 core samples. Porosity ranges from 0.69% to 21.45% with an average of 8.35% (Figure 10(a)), and the horizontal air permeability ranges from 0.006 mD to 8.42 mD with an average of 0.67 mD (Figure 10(b)). Approximately 79.21% of the 1188 core sandstone samples of the Lower Shihezi Formation are tight sandstones with permeabilities of less than 1 mD, with only eight core samples having permeabilities higher than 8 mD, which is likely related to microfractures and strong dissolution. Overall, porosity and permeability show a positive correlation (Figure 11).

4.3.2. Pore Types and Characteristics. Based on observations of thin sections and SEM, the pore types include intergranular dissolved micropores (Figures 12(a), 12(c), 13(c), 13(e), and 13(f)), intragranular dissolved micropores (Figures 12(a)–12(c)), micropores in clay minerals and mineral grains (Figures 13(a) and 13(b)), and microfractures (Figures 12(d) and 13(d)). These tight gas sandstones also feature a wide range of pore sizes (Figures 13 and 14) ranging from the maximum pore size of 0.54 mm to the minimum of 10 μm. The micro- and nanopores, which are developed in intergrain minerals as pore filling matrix due to diagenesis or dissolution, are the key storage spaces for the tight gas sandstones. Based on the MICP curves of the 136 core samples, the maximum pore throat size ranges from 0.035 to 13.29 μm, 94.12% are less than 5 μm (Figure 14(a)), and 97.79% of the pore throats are less than 1 μm (Figure 13(b)).

The tight sandstone reservoirs were divided into three types based on capillary pressure curves and pore throat radius distributions (Figure 15). Type I usually has low displacement pressure (< 0.1 MPa), low median pressure (1-3 MPa), and large pore throat (0.16-2.5 μm) size. And the sandstones have good reservoir quality and are the best reservoirs. Type II usually has low displacement pressure (< 1 MPa), high median pressure (20-50 MPa), and small pore throat (< 1 μm) size. This type sandstones are mainly

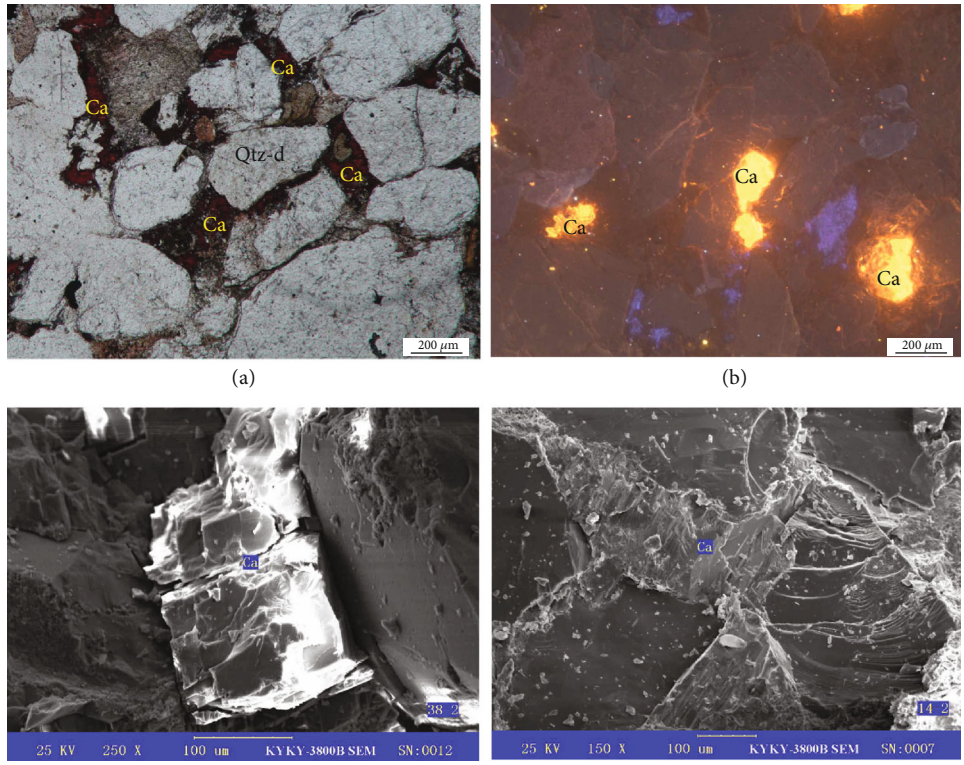

FIGURE 9: Photomicrograph showing calcite. (a) Micrograph of thin section showing calcite, well J97, 2334.86 m. (b) CL micrograph showing the calcite (reddish orange luminescent), well J114, 3006.63 m. (c) Micrograph of SEM showing the calcite, well J78, 3102.05 m. (d) Micrograph of SEM showing the pore-filling calcite, well J77, 2690.2 m.

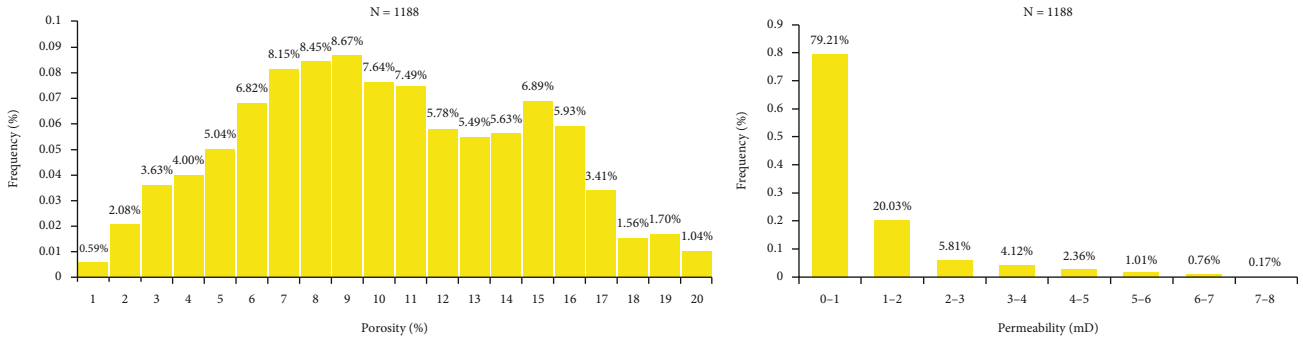

FIGURE 10: Porosity and permeability distribution of the tight sandstone.

fine sandstones. Type III has the highest displacement pressure (> 10 MPa), and the maximum mercury saturation is less than 50% (Figure 15). That means this type sandstones cannot be reservoirs. In general, the capillary pressure curves of type I generally show a platform with left concave shape (Figure 15), but the capillary pressure curves of the type II and III are steep or have right convex shapes (Figure 15). The course-grained sandstones and some medium-grained sandstones usually have the type I pore type. The sandy conglomerates and some mediun-grained sandstones mainly have the type II pore type. And the fine-grained sandstone has type III pore type (Figure 15).

5. Discussion

5.1. Diagenetic Sequence. According to the national standards of the Oil and Gas Industry in China (SY/T5477-2003), the diagenetic stage was divided to eodiagenesis (A and B subage stage), mesodiagenesis (A and B subage stage), and telodiagenesis according to vitrinite reflectance (Ro), homogenization temperature of the aqueous inclusions, petrographic evidence including evolution degree of clay minerals (mixed-layer illite/smectite), crosscutting relationships of cements, and dissolution-filling relationships of diagenetic minerals and pore types.

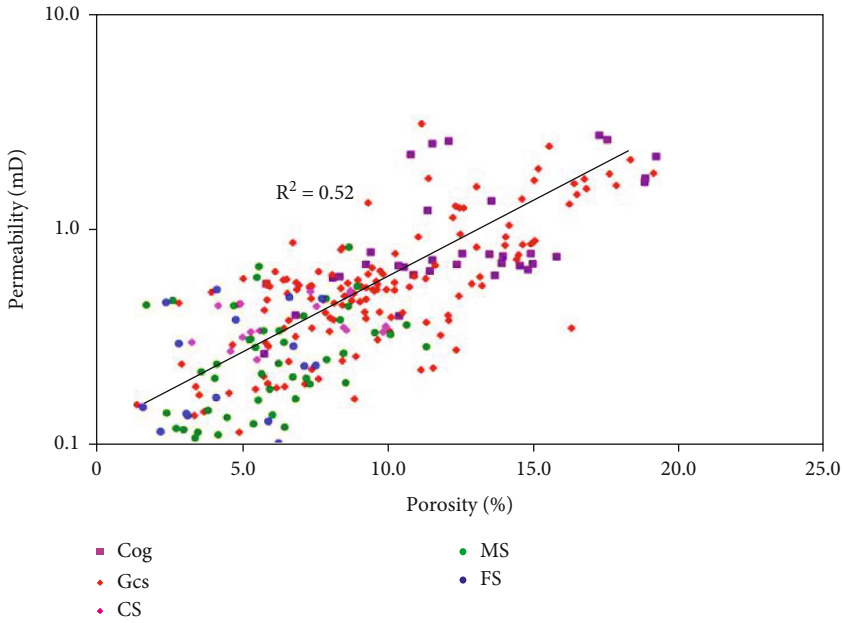

Figure 11: Scatter diagram of the relationship between porosity and permeability of sandstone with different grain size. Key: Cog: conglomerate; Gcs: gravelly coarse sandstone; CS: coarse sandstone; MS: medium sandstone; FS: fine sandstone (FS).

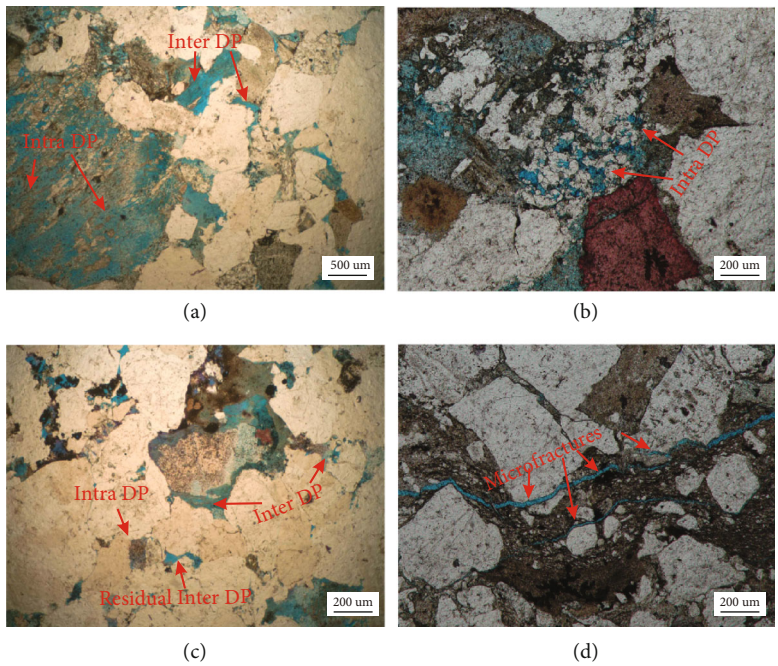

Figure 12: Micrograph of thin section showing the pore types. (a) Intergranular dissolved micropores and intragranular dissolved micropores (intra DP), well J105, 2246.5 m. (b) Intragranular dissolved micropores, well J91, 2985.02 m. (c) Residual intergranular micropores, J105, 2246.5 m. (d) Microfractures, J72, 2987.73 m.

Chlorite coatings are commonly developed around quartz grains where there usually have remaining pores and no quartz cements, which indicates that chlorite formed before quartz cement and strong compaction (Figures 8(d) and 10(a)). The type I quartz cementation of quartz overgrowth (stage-I quartz cement, Figure 8(a)) is earlier than the type II of authigenic quartz (stage-II quartz cement, Figure 8(d)). During the eodiagenesis A stage, the sediment underwent a rapid settling process after deposition (Figure 3). In this process, the sandstone is strongly compacted, and the reservoir primary pore space is rapidly reduced. And the coating chlorites and stage-I quartz cements were formed at the stage. During the eodiagenesis B, the maximum burial depth is around 2000 m. The ground temperature reaches 65°C to

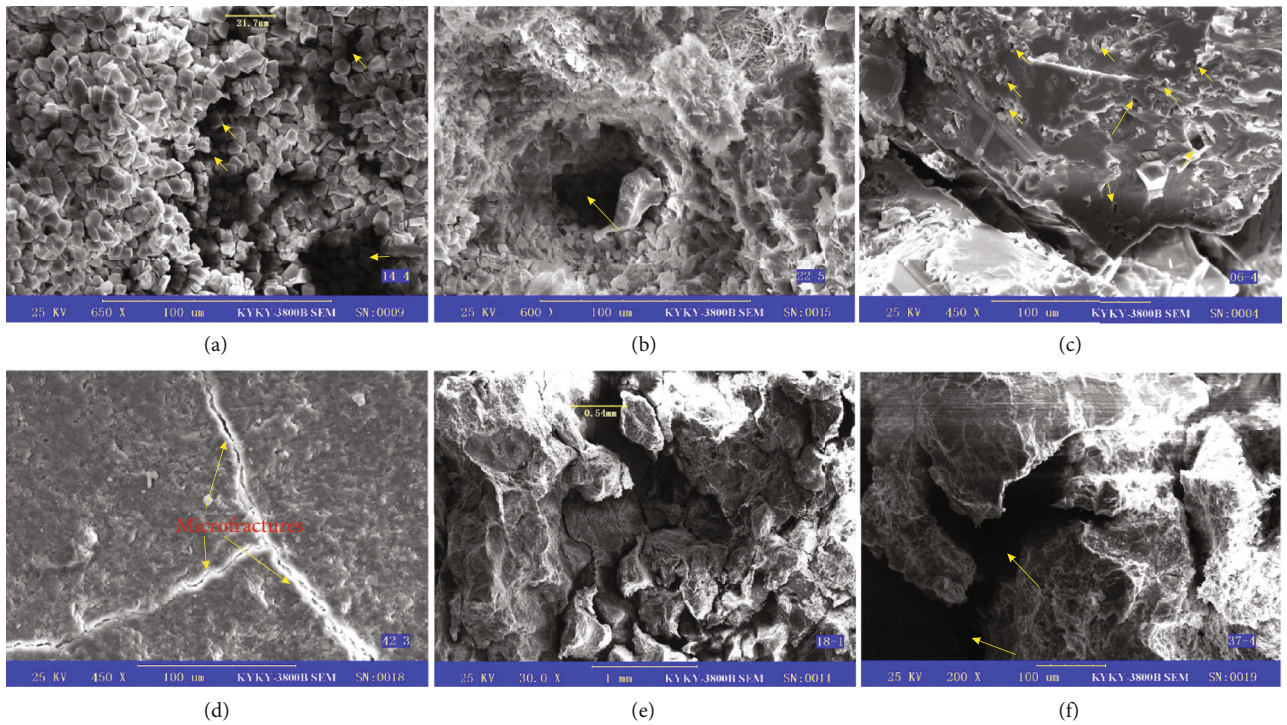

Figure 13: Micrograph of SEM showing the pore-throat types and characteristics. (a) Micropores in authigenic kaolinites, well J77, 2690.2 m. (b) Intragranular dissolved micropores of clay minerals, well J77, 2692.57 m. (c) Intragranular dissolved micropores of quartz detrital grain, well J89, 3082.34 m. (d) Microfractures, well J2, 3066.1 m. (e) Intergranular dissolved micropores, well J89, 3087.05 m. (f) Intergranular dissolved micropores good connectivity, well J77, 2692.57 m. The yellow arrow points to the micropore or microfractures.

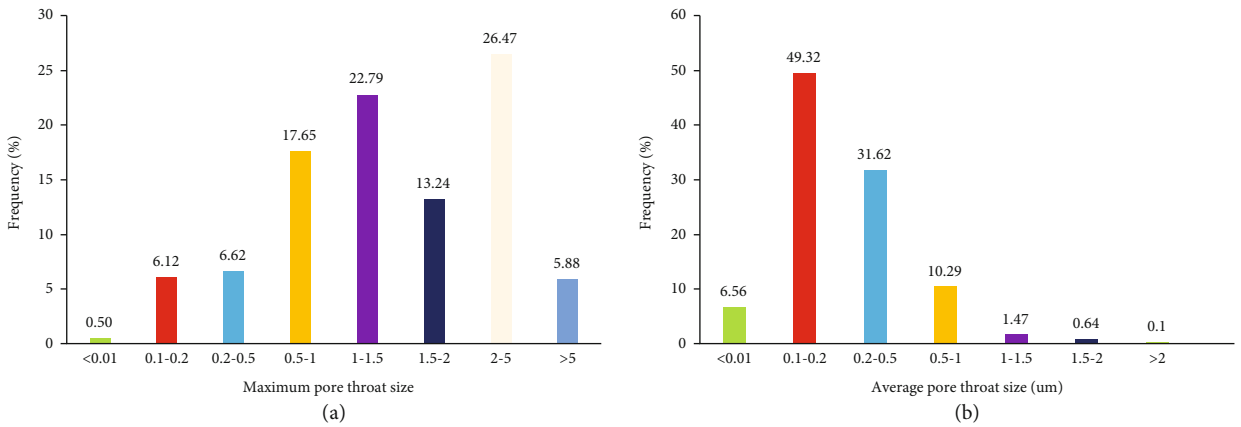

Figure 14: Pore throat size distribution (μm).

85°C, and organic matter begins to produce organic acids, causing dissolution of feldspars and rock chips in the reservoir. And the resulting dissolution products, such as quartz, kaolinite, and calcite, are further cemented to fill the reservoir pores. During the mesodiagenesis A stage, the maximum burial depth is around 2000 m, and the ground temperature reaches 130°C; organic matter produces large amounts of organic acids to dissolve feldspars and rock chips, forming dissolution pores and at the same time, the dissolution products become colloidal to form colloidal materials such as quartz and iron calcite (Figures 3 and 16). Therefore, the main diagenetic progresses that tight sandstones experienced include mechanical compaction, chlorite coating, stage-I quartz cement, chemical compaction, dissolution, stage-II quartz cement, and calcium pore-filling cementation. The burial depth of the tight sandstones of the Lower Shihezi Formation is generally 2600-3300 m. The vitrinite reflectance value of the Lower Shihezi Formation ranges from 1.01% to 1.27%. The homogenization temperature of the aqueous inclusions ranges from 90°C to 130°C [32]. The percentage of S in I/S is 15-26% indicating that the illite/montmorillonite interlayer minerals are highly ordered illite among the clay

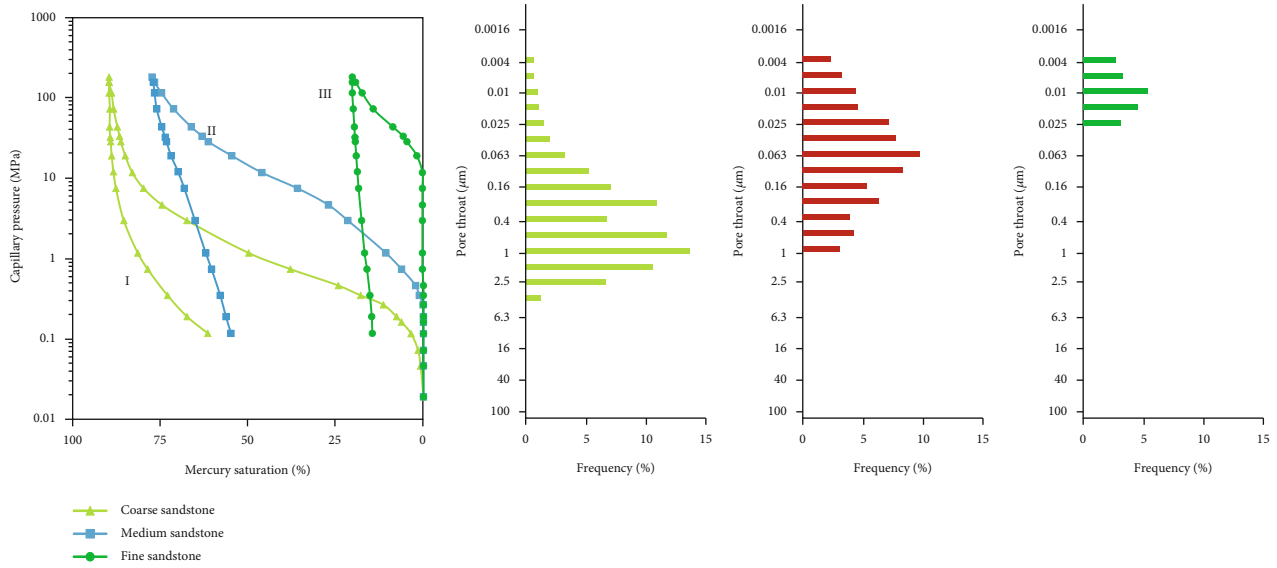

Figure 15: Typical capillary curves and pore throat distribution.

Stage	Eodiagenesis		Mesodiagenesis		Telodiagenesis
	A	B	A	B	
Temperature (°C)	<65	65–85	85–140	140–175	175–200
Ro (%)	<0.35	0.35–0.5	0.5–1.3	1.3–2.0	2.0–4.0
I/S (%)	>70	70–50	50–15	<15	Absent
Mechanical compaction					
Mechanical compaction					
Chlorite coating					
Quartz cement					
Dissolution					
Carbonate cement					
Authigenic clay: Illite/smectite					
Authigenic clay: Kaolinite					
Authigenic clay: Illite					
Authigenic clay: Chlorite					

Figure 16: Diagenetic sequence of Lower Shihezi Formation tight sandstone. The width of the symbols represents the relative occurring rate of the authigenic minerals.

minerals of sandstone. In summary, the Lower Shihezi Formation is in the mesodiagenesis A substage to mesodiagenesis B substage (Figure 15).

5.2. Diagenetic Controls on Reservoir Quality

5.2.1. Compactional Controls on Reservoir Quality. Compaction occurred widely in the Lower Shihezi sandstones (Figure 5). A quantitative evaluation of intergranular volume (IGV) was used to clarify the compaction and cementation impacts on Lower Shihezi tight sandstone reservoir quality.

Firstly, the recovery of the original porosity is mainly based on the relationship between sandstone sorting coefficient and original porosity proposed by Beard and Weyl [39].

$$\Phi 0 = \frac{20.9 + 22.91}{\mathrm{So}}, \tag{1}$$

where $\Phi 0$ is the original porosity, and So is the sandstone sorting coefficient.

Table 2: Relationship between reservoir diagenesis and pore evolution.

Sample	So	C	$\varphi 0$ (%)	$\varphi 1$ (%)	$\varphi 2$ (%)	$\varphi 3$ (%)	$\varphi 4$ (%)	Original porosity destroyed by mechanical compaction (%)	Original porosity destroyed by cementation (%)
S1	1.89	2.36	33.03	8.85	6.49	3.32	9.81	73.21	7.15
S2	2.01	4.60	32.30	6.39	1.79	3.52	5.31	80.21	14.24
S3	1.85	6.32	33.29	7.88	1.56	2.54	4.10	76.33	18.99
S4	1.78	7.35	33.78	9.69	2.34	2.78	5.12	71.32	21.76
S5	2.21	8.45	31.27	9.55	1.10	3.45	4.55	69.45	27.02
S6	1.79	8.65	33.70	15.06	6.41	3.22	9.63	55.33	25.67
S7	1.93	8.93	32.78	12.34	3.41	3.19	6.60	62.34	27.25
S8	1.86	9.32	33.22	12.21	2.89	4.22	7.11	63.25	28.05
S9	2.11	7.56	31.76	8.80	1.24	1.43	2.67	72.31	23.80
S10	1.77	10.16	33.85	15.34	5.18	1.78	6.96	54.67	30.02
S11	2.04	10.33	32.14	12.11	1.78	3.89	5.67	62.33	32.15
S12	2.13	6.77	31.66	10.64	3.87	5.21	9.08	66.38	21.38
S13	1.75	8.43	34.00	10.76	2.33	5.77	8.10	68.34	24.80
S14	1.87	14.87	33.16	16.13	1.26	2.78	4.04	51.35	44.85
S15	1.88	14.88	33.09	19.37	4.49	3.98	8.47	41.45	44.97
S16	1.92	14.92	32.84	22.36	7.44	5.12	12.56	31.92	45.44
S17	1.94	14.94	32.71	20.34	5.40	4.23	9.63	37.81	45.67
S18	1.99	14.99	32.42	16.42	1.43	4.11	5.54	49.34	46.24
S19	2.04	15.04	32.14	15.17	0.13	4.56	4.69	52.78	46.80
S20	2.07	12.07	31.97	13.47	1.40	3.55	4.95	57.88	37.75
S21	1.97	13.22	32.53	14.90	1.68	5.77	7.45	54.21	40.63
S22	2.19	17.34	31.37	18.09	0.75	4.88	5.63	42.32	55.28
S23	1.88	14.45	33.09	17.83	3.38	6.02	9.40	46.11	43.67
S24	1.84	20.11	33.36	20.94	0.83	3.78	4.61	37.22	60.29
S25	1.76	20.21	33.92	26.40	6.19	3.98	10.17	22.18	59.58

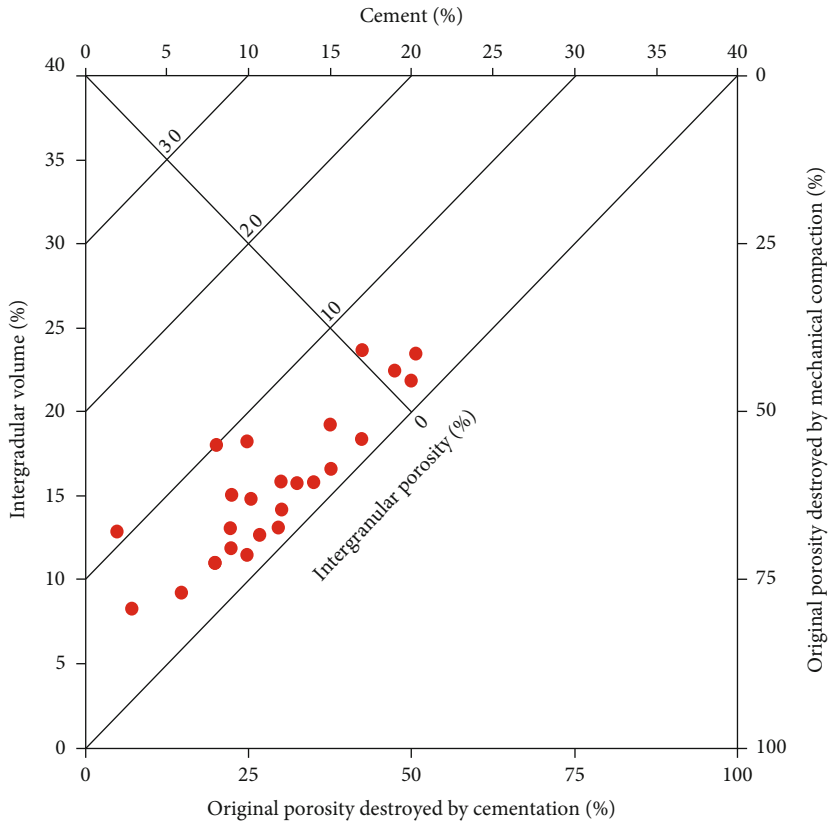

Figure 17: Intergranular volume (IGV) versus volume of cements (based on Houseknecht [40]; Ehrenberg [41]).

The current pore volume is formed by the further reduction of the remaining intergranular pore volume and the increase of some small pore volume after cementation. Therefore, the residual porosity after compaction can be calculated as following:

$$\Phi 1 = \frac{C + (P1 + P2) \times P3}{P4}, \tag{2}$$

where $\Phi 1$ is the residual porosity after compaction, C is the content of cementation, P1 is the measured intergranular porosity, P2 is the measured microporous surface porosity based the thin section, P3 is the air measurement porosity, and P4 is the total pore surface porosity.

$$\Phi 2 = \Phi 1 - C, \tag{3}$$

where $\Phi 2$ is the residual porosity after cementation.

$$\Phi 3 = \frac{P5 \times P3}{P4}, \tag{4}$$

where $\Phi 3$ is the porosity increased by dissolution, and P5 is the dissolution surface porosity based on the thin section.

$$\Phi 4 = \Phi 2 + \Phi 3, \tag{5}$$

where $\Phi 4$ is the calulated current porosity.

Based on the above equations, the porosity evolution of 30 wells in the study area was quantified, and the results were calculated as follows (Table 2). IGV values range from 8.4% to 24.3% (Figure 17). The primary porosity of the Lower Shihezi sandstone reservoirs was mainly destroyed by mechanical compaction, and the cementation destroyed primary porosity less than 33% vol % (Figure 17). The mechanical compaction accounted for 44.2%–79.81% (with an average of 61.32%) of the total intergranular pore volume loss (PVL) during burial (an initial porosity of 34% calculated based on the Beard and Weyl, 1973).

5.2.2. Clay Mineral Cement Control on Reservoir Quality. The clay mineral cements have significant effect on Lower Shihezi sandstone pore and throat size distributions (Figures 5 and 11). The pore throat systems primarily control the porosity and permeability of the tight sandstone resulting in positive correlation between porosity and permeability [42, 43]. The correlation coefficient between porosity and permeability in the Lower Shihezi tight sandstone reservoirs is about 0.52 (Figures 10 and 11) as the result of the clay cementation, but the different kinds of clay mineral cements have different effects on tight sandstone porosities. The relationship between I/S, kaolinite, illite content, and porosity and permeability show that the porosity and permeability decrease with the increase of these mineral cements (Figures 18(a)–18(f)). The inverse correlation suggests that these three types of clay mineral cements occlude both pores and pore throats, but the relationship between

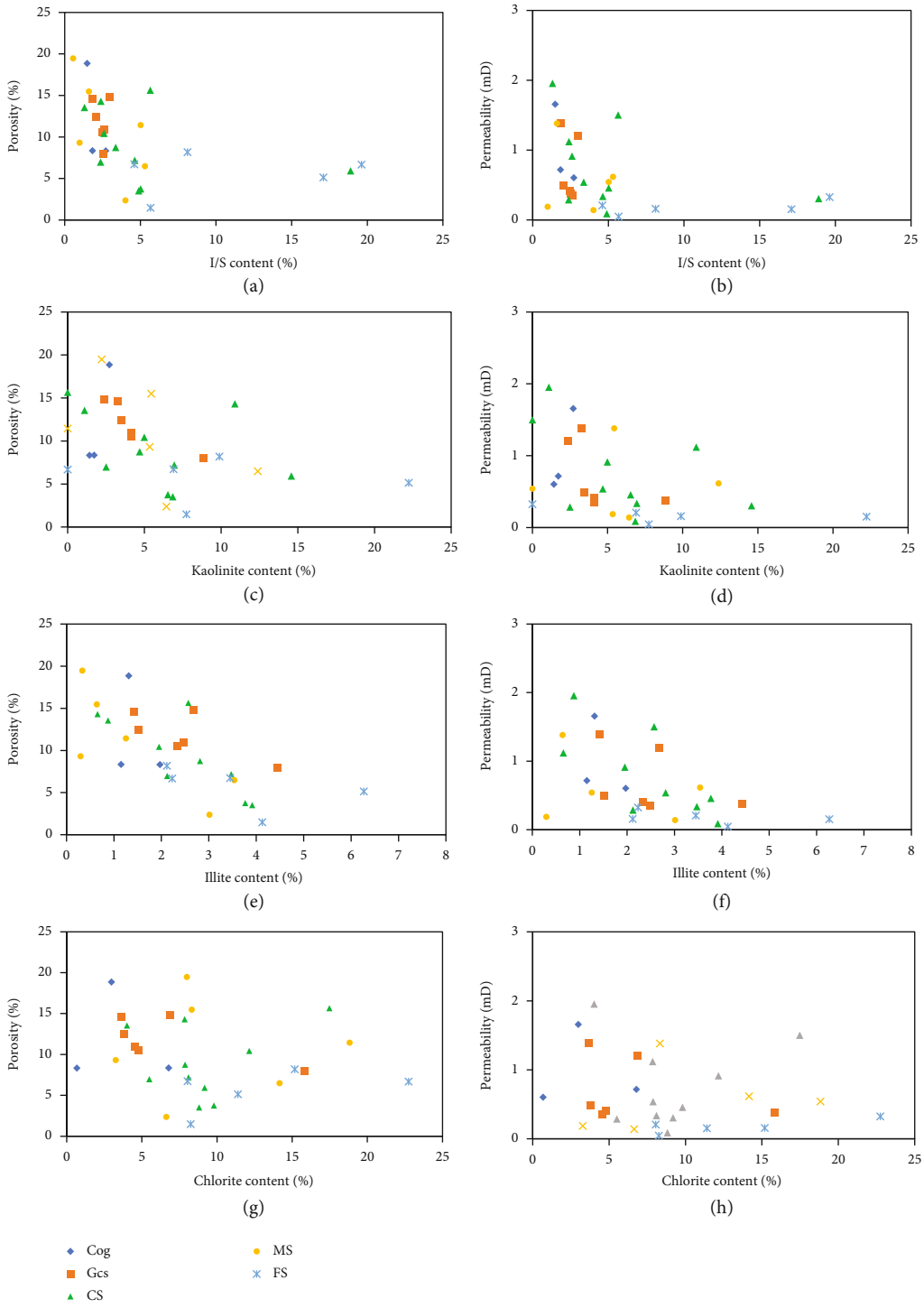

FIGURE 18: The relationship of clay minerals and reservoir quality [15]. Key: Cog: conglomerate; Gcs: gravel bearing coarse sandstone; CS: coarse sandstone; MS: medium sandstone; FS: fine sandstone.

chlorite content and porosity shows that porosity decreases with the content of chlorite less 10%, and then when the chlorite content is greater than 10%, the porosity becomes larger as the chlorite content increases (Figure 18(g)). This implies that chlorite coatings have preserved the porosity from quartz overgrowth as show in Figure 7(e), that reducing of pore space due to cementation. In contrast, permeability decreases as the chlorite content increases (Figure 18(h)). This indicates that, despite the chlorite coating effect of preserving porosity, the pore-lining chlorites may significantly obstruct pore throats.

5.3. Depositional Impacts on Diagenesis and Reservoir Quality. The Permian Lower Shihezi Formation was deposited in a

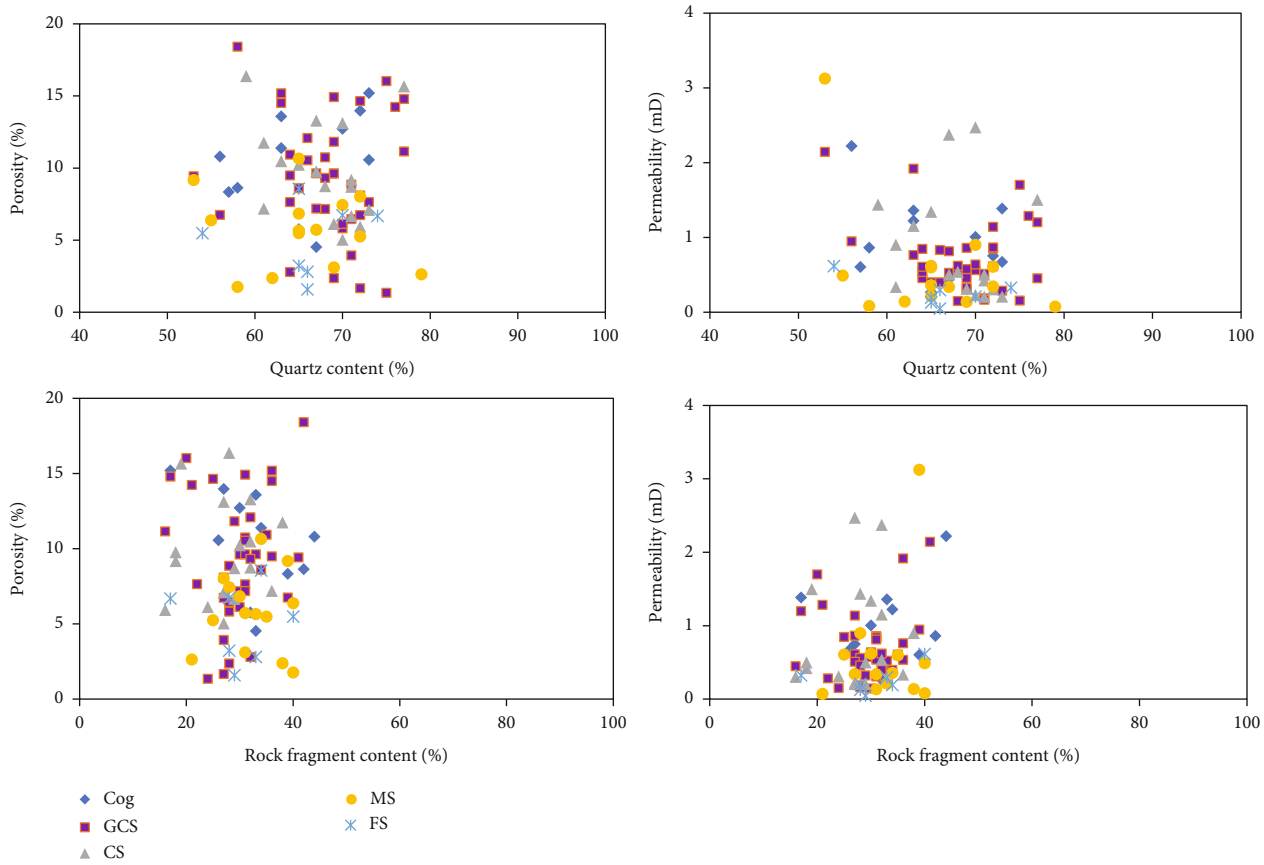

Figure 19: The relationship of quartz content and rock fragment content with reservoir quality.

warm and humid climate by braided river systems [17, 18], and all Lower Shihejie tight sandstones share similar depositional environments. There is no obvious relationship between the content of the quartz and rock fragments and reservoir quality (Figure 19). With an increase of quartz content or rock fragments, porosity and permeability show no increase or decrease. However, data from this study suggests that tight sandstone granularity shows some effect. In the study area, the coarser sandstones (Cog, Gcs, CS) have better reservoir quality than the medium and fine sandstones [44] (Figures 10 and 14). We interpret that this is caused by higher discharge during the deposition of the coarser sandstones, which can flush the clay and siltstone away resulting in less cementation.

6. Conclusions

(1) The sandstones of Lower Shihezi are mostly litharenite and minor sublitharenite and feldspathic litharenite, which are characterized by abundant quartz

(2) The Lower Shihezi sandstones have ultralow porosity and permeability, small pore throats, and high displacement pressures. The pore types include intergranular dissolved micropores, intragranular dissolved micropores, micropores in clay minerals and mineral grains, and microfractures. The tight sandstones were divided into three types based on capillary pressure curves and pore throat radius distributions, which the type I sandstones are the best reservoirs

(3) The Lower Shihezi tight sandstone reservoirs have undergone complex diagenetic alteration. Compaction and clay mineral cements are the two crucial diagenetic factors that controlled the tightness of the reservoirs. The compaction has destroyed most of primary porosity, and the effective pores are mainly dissolved micropores, intragranular dissolved micropores, and micropores in clay minerals and mineral grains. The chlorite coating might help preserve certain amount of porosity, but pore-lining chlorites significantly obstruct pore throats and reduce permeability

Data Availability

All data supporting the results of this study are presented in this paper.

Conflicts of Interest

The authors declare that they have no conflicts of interest.

Acknowledgments

The research was supported by the Natural Science Foundation of Hubei Province China (Grant No. 2019CFB341), Educational Commission of Hubei Province of China (Grant No. Q20211306), and the Ningxia Natural Science Foundation Project (Grant No. 2021AAC05024). We thank the North China Bureau of Petroleum, SINOPEC for providing data.

References

[1] I. Becker, P. Wüstefeld, B. Koehrer, M. Felder, and C. Hilgers, "Porosity and permeability variations in a tight gas sandstone reservoir analogue, Westphalian D, Lower Saxony Basin, NW Germany: influence of depositional setting and diagenesis," *Journal of Petroleum Geology*, vol. 40, no. 4, pp. 363–389, 2017.

[2] G. Thyne, "A model for diagenetic mass transfer between adjacent sandstone and shale," *Marine and Petroleum Geology*, vol. 18, no. 6, pp. 743–755, 2001.

[3] S. Gier, R. H. Worden, W. D. Johns, and H. Kurzweil, "Diagenesis and reservoir quality of Miocene sandstones in the Vienna Basin, Austria," *Marine and Petroleum Geology*, vol. 25, no. 8, pp. 681–695, 2008.

[4] K. Bjørlykke and J. Jahren, "Open or closed geochemical systems during diagenesis in sedimentary basins: constraints on mass transfer during diagenesis and the prediction of porosity in sandstone and carbonate reservoirs," *AAPG Bulletin*, vol. 96, no. 12, pp. 2193–2214, 2012.

[5] G. Yuan, J. Gluyas, Y. Cao et al., "Diagenesis and reservoir quality evolution of the Eocene sandstones in the northern Dongying sag, Bohai Bay basin, East China," *Marine and Petroleum Geology*, vol. 62, pp. 77–89, 2015.

[6] B. E. Law and J. B. Curtis, "Introduction to unconventional petroleum systems," *AAPG Bulletin*, vol. 86, pp. 1851-1852, 2002.

[7] M. A. Islam, "Diagenesis and reservoir quality of Bhuban sandstones (Neogene), Titas gas field, Bengal Basin, Bangladesh," *Journal of Asian Earth Sciences*, vol. 35, no. 1, pp. 89–100, 2009.

[8] C. N. Zou, R. K. Zhu, K. Y. Liu et al., "Tight gas sandstone reservoirs in China: characteristics and recognition criteria," *Journal of Petroleum Science and Engineering*, vol. 88-89, pp. 82–91, 2012.

[9] M. A. Arthur and D. R. Cole, "Unconventional hydrocarbon resources: prospects and problems," *Elemenstylolitests*, vol. 10, no. 4, pp. 257–264, 2014.

[10] A. Fall, P. Eichhubl, R. J. Bodnar, S. E. Laubach, and J. S. Davis, "Natural hydraulic fracturing of tight-gas sandstone reservoirs, Piceance Basin, Colorado," *Geological Society of America Bulletin*, vol. 127, no. 1-2, pp. 61–75, 2015.

[11] J. X. Dai, Y. Y. Ni, and X. Q. Wu, "Tight gas in China and its significance in exploration and exploitation," *Petroleum Exploration and Development*, vol. 39, no. 3, pp. 277–284, 2012.

[12] M. J. J. Rahman and T. Mccann, "Diagenetic history of the Surma group sandstones (Miocene) in the Surma Basin, Bangladesh," *Journal of Asian Earth Sciences*, vol. 45, pp. 65–78, 2012.

[13] T. M. Stroker, N. B. Harris, and W. C. Elliott, "Diagenesis of a tight gas sand reservoir: Upper Cretaceous Mesaverde Group, Piceance Basin, Colorado," *Marine and Petroleum Geology*, vol. 40, pp. 48–68, 2013.

[14] K. Xi, Y. Cao, J. Jahren et al., "Diagenesis and reservoir quality of the Lower Cretaceous Quantou Formation tight sandstones in the southern Songliao Basin, China," *Sedimentary Geology*, vol. 330, pp. 90–107, 2015.

[15] R. Wang, W. Shi, X. Xie et al., "Clay mineral content, type, and their effects on pore throat structure and reservoir properties: insight from the Permian tight sandstones in the Hangjinqi area, North Ordos Basin, China," *Marine and Petroleum Geology*, vol. 115, article 104281, 2020.

[16] C. Zou, R. Zhu, S. T. Wu et al., "Types, characteristics, genesis and prospects of conventional and unconventional hydrocarbon accumulations: taking tight oil and tight gas in China as an instance," *Acta Petrolei Sinica*, vol. 33, pp. 173–187, 2012.

[17] W. T. Dou, M. C. Hou, and G. Y. Dong, "Provenance analysis of the Upper Paleozoic Shanxi to Lower Shihezi formations in North Ordos Basin," *Natural Gas Industry*, vol. 29, pp. 25–28, 2009.

[18] J. X. Qiao, H. Deng, C. Y. Liu, H. G. Zhao, and H. R. Wang, "Sedimentary-tectonic framework and provenance analysis of the late Paleozoic in the northern Ordos Basin," *Journal of Xi'an Shiyou University (Natural Science Edition)*, vol. 28, pp. 12–17, 2013.

[19] A. Q. Chen, H. D. Chen, M. C. Hou, S. L. Xu, C. G. Zhang, and J. Wang, "Late Paleozoic sedimentary filling and gas accumulation in the North Ordos Basin," *Earth Sciences- Journal of China University of Geosciences*, vol. 37, pp. 151–162, 2012.

[20] I. P. Montanez, "Secondary porosity and late diagenetic cements of the Upper Knox Group, Central Tennessee region. A temporal and spatial history of fluid flow conduits development within the Knox regional aquifer," in *Basin-wide diagentic patterns*, I. P. Montanez, J. M. Gregg, and K. L. Shelton, Eds., pp. 101–117, Integrated petrologic, Geochemical and Hydrological Considerations: SEPM Special Publication, 1997.

[21] F. Liu, W. Zhou, X. Li, R. Xie, and L. Li, "Analysis of characteristics of the clay minerals in the upper palaeozoic sandstone reservoir of Hangjinqi area in North Ordos Basin," *Journal of Mineral Petrology*, vol. 26, pp. 92–97, 2006.

[22] D. Xiao and Q. Fu, "The genetic mechanism of authigenic quartz in Lower Shihezi Formation of Hanggin Banner, northern Ordos Basin," *Acta Petrologica et Mineralogica*, vol. 30, pp. 113–120, 2011.

[23] L. Qiu, X. Mu, H. Li, J. Zhang, Y. Qiao, and S. Zhou, "Influence of diagenesis of tight sandstone reservoir on the porosity development of lower Shihezi formation in Hangjinqi area, Ordos Basin," *Petroleum Geology and Recovery Efficiency*, vol. 26, pp. 42–50, 2019.

[24] X. Q. Ding, S. N. Zhang, W. Zhou, L. Z. Deng, and X. H. Li, "Characteritics and genesis of the Upper Paleozoic tight sandstone reservoirs in the northern Ordos Basin," *Oil and Gas Geology*, vol. 28, pp. 491–496, 2007.

[25] J. L. Luo, X. S. Liu, X. Y. Fu, M. Li, R. Kang, and Y. N. Jia, "Impact of petrologic components and their diagenetic evolution on tight sandstone reservoir of Upper Paleozoic in northern Ordos Basin," *Earth Science-Journal of China University of Geosciences*, vol. 39, pp. 537–545, 2014.

[26] M. H. Yang, L. Li, J. Zhou et al., "Mesozoic structural evolution of the Hangjinqi area in the northern Ordos Basin, North China," *Marine and Petroleum Geology*, vol. 66, pp. 695–710, 2015.

[27] Z. L. Zhu, W. H. Li, K. Y. Li, Q. H. Chen, Y. Q. Guo, and Z. Yuan, "The characteristic of sequence stratigraphy and sedimentary systems of Taiyuan-Xiashihezi Formation in Hangjinqi area," *Journal of Northwest University*, vol. 30, pp. 1050–1054, 2010.

[28] C. N. Zou, X. Y. Zhang, P. Luo, L. Wang, Z. Luo, and L. H. Liu, "Shallow-lacustrine sand-rich deltaic depositional cycles and sequence stratigraphy of the Upper Triassic Yanchang formation, Ordos Basin, China," *Basin Research*, vol. 22, no. 1, pp. 108–125, 2010.

[29] M. Yang, L. Li, J. Zhou, X. Qu, and D. Zhou, "Segmentation and inversion of the Hangjinqi fault zone, the northern Ordos basin (North China)," *Journal of Asian Earth Sciences*, vol. 70-71, pp. 64–78, 2013.

[30] M. H. Yang and C. Y. Liu, "Sequence stratigraphic framework and its control on accumulation of various energy resources in the Mesozoic continental basins in Ordos," *Oil and Gas Geology*, vol. 27, pp. 563–570, 2006.

[31] X. Q. Zheng and G. Yan, "Types of hydrocarbon traps in Hangjinqi area of northern Ordos Basin," *Progress in Exploration Geophysics*, vol. 29, pp. 279–284, 2006.

[32] H. Xue, J. Zhang, Y. Wang, B. Xu, and H. Guo, "Relationship between tectonic evolution and hydrocarbon in Hangjinqi block of North Ordos basin," *Geotectonica et Metallogenia*, vol. 2, p. 003, 2009.

[33] H. Xue, Y. Wang, X. Mao et al., "The timing of gas pooling in the upper Paleozoic in the northern Ordos Basin: a case study of the Hangjinqi block," *Natural Gas Industry*, vol. 29, pp. 9–12, 2009.

[34] Y. Yang, W. Li, and L. Ma, "Tectonic and stratigraphic controls of hydrocarbon systems in the Ordos basin: a multicycle cratonic basin in Central China," *AAPG Bulletin*, vol. 89, no. 2, pp. 255–269, 2005.

[35] G. P. Zhao, "Characterization of fluid inclusions and timing of gas accumulation in Upper Paleozoic reservoirs of Hangjinqi area, Ordos Basin," *Oil and Gas Geology*, vol. 38, no. 5, pp. 905–912, 2017.

[36] C. Zhang, H. Luo, C. Zhang et al., "Diagenesis and porosity evolution model of the quartzose sandstone reservoir with moderate palaeogeothermal, long period of large buried-depth: a case form the Lower Shihezi Reservoir in Yan'an, Ordos Basin," *Advances in Earth Science*, vol. 32, pp. 744–756, 2017.

[37] F. L. Folk, *Petroleum of Sedimentary Rocks*, Hempill's, Austin Texas, 1968.

[38] H. Gao and H. A. Li, "Pore structure characterization, permeability evaluation and enhanced gas recovery techniques of tight gas sandstones," *Journal of Natural Gas Science and Engineering*, vol. 28, pp. 536–547, 2016.

[39] D. C. Beard and P. K. Weyl, "Influence of texture on porosity and permeability of unconsolidated sand," *AAPG Bulletin*, vol. 57, no. 2, pp. 349–369, 1973.

[40] W. D. Houseknecht, "Assessing the relative importance of compaction processes and cementation to reduction of porosity in sandstones," *AAPG Bulletin*, vol. 71, pp. 633–642, 1987.

[41] S. N. Ehrenberg, "Assessing the relative importance of compaction processes and cementation to reduction of porosity in sandstones: Discussion; compaction and porosity evolution of Pliocene sandstones, Ventura Basin, California: DISCUSSION," *AAPG Bulletin*, vol. 73, 1989.

[42] P. H. Nelson and J. E. Kibler, "Permeability-porosity relationships in sedimentary rocks," *Logic and Analysis*, vol. 35, pp. 38–62, 1994.

[43] J. Lai, G. W. Wang, Z. Y. Fan, Z. L. Zhou, J. Chen, and S. C. Wang, "Fractal analysis of tight shaly sandstones using nuclear magnetic resonance measurements," *AAPG Bulletin*, vol. 102, no. 2, pp. 175–193, 2018.

[44] R. Xie, W. Zhou, L. Li, Y. Su, and X. Wang, "Characteristics of upper Paleozoic sandstone reservoir in Hangjinqi area of Ordos Basin," *Xinjiang Geology*, vol. 28, pp. 86–90, 2010.